J Vis (2010) 13:251–256
DOI 10.1007/s12650-010-0035-0

REGULAR PAPER

**V. G. Chernoray · A. V. Dovgal · V. V. Kozlov · L. Löfdahl**

# Secondary instability of a swept-wing boundary layer disturbed by controlled roughness elements

Received: 9 December 2009 / Accepted: 28 March 2010 / Published online: 17 April 2010


**Abstract** Wind-tunnel data on velocity perturbations evolving in a laminar swept-wing flow under low subsonic conditions are reported. The focus of the present experiments are secondary disturbances of the boundary layer which is modulated by stationary streamwise vortices. Both the stationary vortices and the secondary oscillations of interest are generated in a controlled manner. The experimental data are obtained through hot-wire measurements. Thus, evolution of the vortices, either isolated or interacting with each other, is reconstructed in detail. As is found, the secondary disturbances, initiating the laminar-flow breakdown, are strongly affected by configuration of the stationary boundary-layer perturbation that may have an implication to laminar–turbulent transition control.

**Keywords** Swept wing · Streamwise vortices · Secondary instabilities · Transition control

## 1 Introduction

A number of research data on transition to turbulence in shear layers testify to the laminar-flow breakdown initiated by 3D perturbations appearing as streamwise vortices and, so called, streaky structures. Modulating the base flow, they generate local regions of strong velocity gradients. As a result, high-frequency (secondary) instabilities start to grow dominating the laminar–turbulent transition. In 2D boundary layers and channel flows, such a path of the transition was previously observed by Elofsson et al. (1999), Matsson and Alfredsson (1990) and Matsubara and Alfredsson (2001).

Similarly, a swept-wing boundary layer with a 3D flow pattern in the near-wall region is primarily unstable to stationary crossflow vortices which induce amplifying secondary oscillations. A series of experiments have been performed on this topic under natural and controlled conditions of the flow instability (Poll 1979; Nitschke-Kowsky and Bippes 1988; Kohama et al. 1991; Kohama et al. 1996; Deyhle and Bippes 1996; Kawakami et al. 1999; Boiko et al. 2000; Kozlov et al. 2001; White et al. 2001; White and Saric 2005). The wind-tunnel data of the above references supported an idea on the secondary perturbations originating locally from strong shear induced in the swept-wing flow by the crossflow vortices (Kohama et al. 1991). Also, amplitude characteristics of the oscillations riding on the primary vortices were made

V. G. Chernoray · L. Löfdahl
Chalmers University of Technology, 412 96 Göteborg, Sweden

A. V. Dovgal (✉) · V. V. Kozlov
Khristianovich Institute of Theoretical and Applied Mechanics SB RAS, Novosibirsk 630090, Russia
E-mail: dovgal@itam.nsc.ru
Tel.: +7-383-3304278
Fax: +7-383-3307268

clear (Kohama et al. 1996; Kawakami et al. 1999) and linearity of the secondary disturbances at the initial stage of their evolution was confirmed (Boiko et al. 2000).

Further details on the high-frequency perturbations are available from theoretical and numerical work on the secondary instability of swept-wing boundary layers (Fischer and Dallmann 1991; Malik et al. 1999; Janke and Balakumar 2000; Koch et al. 2000; Koch 2002; Högberg and Henningson 1998; Wassermann and Kloker 2002). Along with the experimental findings, the calculation results show that the instability phenomenon under consideration is of much importance during the boundary-layer transition (Högberg and Henningson 1998). An overview of the problem was given recently by Saric et al. (2003).

The present paper focuses on a swept-wing flow, emphasizing its high-frequency disturbances at different spatial arrangements of the stationary vortices embedded in the laminar boundary layer. Particularly, one expects that instability of the laminar flow modulated by the primary vortices is affected by their transverse spacing as it was found through direct numerical simulation (Wassermann and Kloker 2002). To clarify this point experimentally, we examine the stationary vortices and the secondary oscillations, both excited in a controlled manner. The velocity perturbations are investigated by detailed hot-wire measurements, "visualizing" the 3D flow pattern with high spatio-temporal resolution.

## 2 Experimental arrangement

The wind-tunnel results reported in what follows were obtained from the Department of Thermo and Fluid Dynamics, Chalmers University of Technology. The experimental facility has a test section 3-m long, 1.8-m wide and 1.2-m high with the free-stream turbulence level less than 0.1% in the velocity range from 5 to 15 m/s in which the present measurements were performed. The wing model under examination had a C-16 profile with the chord $c = 707$ mm at the sweep angle of 45° and was mounted horizontally, spanning the entire width of the test section (Fig. 1). At the top side of the model, which was a flat one beginning from $0.4c$, the flow was attached to the surface down to the trailing edge of the wing. At the bottom side, the boundary layer was perturbed by a sandpaper strip in the upstream part of the model preventing from flow separation.

Stationary vortices of the laminar boundary layer were generated by roughness elements placed on the wing surface at $0.3c$ from its leading edge. Two elements were used one by one, each of height 0.39 mm, which was close to the local momentum thickness. The first of them was of 35 mm spanwise width and 8 mm length as measured normally to the wing leading edge, producing at its tips a pair of isolated vortices of opposite rotation. In the following, they are denoted as Vortex 1 and Vortex 2. The other roughness element was a circular one of 8 mm in diameter, generating the vortices interacting with each other. Then, high-frequency perturbations evolving along the stationary vortices were excited by periodic suction-blowing through a hole of 0.8 mm in diameter on the surface of the wing. The secondary disturbances, controlled by a remote loudspeaker connected to the hole, were injected in the boundary layer at $0.4c$. In each case under investigation, the spanwise position of the roughness element was adjusted so that the secondary oscillations were excited underneath the primary vortices. Particularly, when comparing Vortices 1 and 2, the elongated element was moved parallel to the wing leading edge, thus, relative position of the vortex generator and the origin of secondary disturbances was the same.

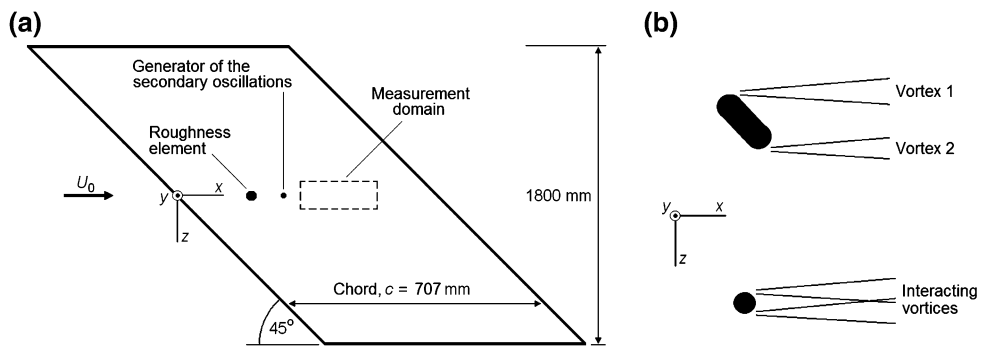


**Fig. 1** Experimental model. **a** Plane view. **b** Elongated and circular roughness elements used for generation of the stationary vortices

The flow pattern was examined through hot-wire measurements with single and V-wire probes calibrated in the free stream against a Pitot-static tube. Typically, the calibration resulted in an error less than 0.5% for all points in the calibration range. The probes were positioned by a computer-controlled traversing mechanism which was completely automated for long experimental runs through definition of a geometrical mesh of measurement points. Equipped with servo-motors, it could sustain an absolute coordinate system with an accuracy of 10 μm in the wing plane and 5 μm normally to the wall. Due to the near-wall effects on the hot-wire data, the latter were not acquired in immediate proximity of the wing surface at the normal-to-wall distance less than about 0.2 and 0.4 mm for single and V-wire probes. For the data acquisition, the IOTech WaveBook 516 sampling module with expansion unit was used, enabling a 16-bit 1 MHz sample and hold with full analog and digital triggering options. Post-processing of the data files was performed in the software package Matlab (Matrix Laboratory, USA).

To observe the secondary perturbations, velocity measurements were phase-locked with the disturbances generator. Each period of the oscillations was resolved with 40 temporal points and ensemble averaging was performed for 50 realizations. From triggered measurements at each point in the spatial domain, one period of the disturbances was obtained so that the velocity field was reproduced in a 4D spatio-temporal matrix $u(x, y, z, t)$. Thus, volumetric flow patterns were created. In what follows, they are shown as iso-surface plots of the stationary mean-velocity perturbation and the nonstationary velocity component taken at a fixed time moment.

The hot-wire results are presented most of all in a wind-tunnel-related coordinate system with the origin of $x$- and $z$-coordinates taken at the wing leading edge, so that $x$-axis is in line with the source of the secondary oscillations and $z$-coordinate is measured transversely in the wing plane (Fig. 1a). At each point of measurements, $y$-axis is normal to $x$–$z$ plane with $y = 0$ at the surface of the model (recall that downstream of $x/c = 0.4$, where the controlled laminar-flow perturbations were recorded, the boundary layer evolved over the flat surface of the wing).

## 3 Wind-tunnel data

The experimental runs were carried out at the oncoming flow velocity $U_0 = 8.2$ m/s corresponding to the chord-based Reynolds number of about 390,000. At first, the unperturbed boundary layer on the wing surface was examined. Then, the streamwise vortices generated by the roughness elements and their secondary instabilities were dealt with.

In the absence of controlled perturbations, a laminar boundary layer develops on the model with the mean flow illustrated in Fig. 2. The velocity distributions measured in the center of the wing span are shown as streamwise ($U_s$) and crossflow ($W_s$) profiles related to the external streamline. Both the components are normalized by local values of the external-flow velocity and the wall-normal coordinate is reduced by the local momentum thickness $\theta$ which is determined by the streamwise velocity component. At $x/c = 0.3$ (Fig. 2a), where the roughness elements were placed afterwards, the accelerating boundary layer with

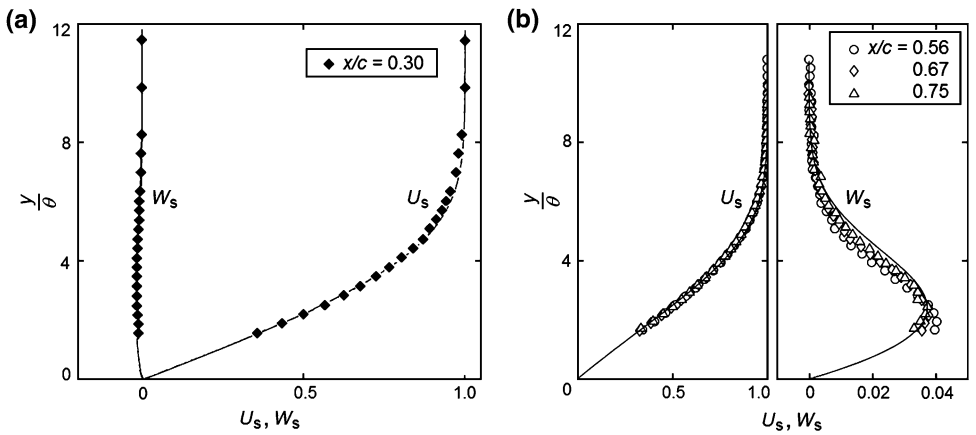


**Fig. 2** Mean-velocity distributions of the unperturbed boundary layer. **a** Velocity profiles measured in the upstream part of the model at $x/c = 0.3$; **b** the same in the downstream sections of the wing; *solid lines* are Falkner–Skan–Cooke similarity solutions

$\theta = 0.31$ mm is well approximated by the Falkner–Skan–Cooke similarity solution at $m = 0.04$ and the external streamline angle of 40.8° as local mean-flow conditions of the stationary vortices generation. Downstream of $x/c = 0.5$ (Fig. 2b), the boundary layer is close to a self-similar one with $m = -0.05$ at the streamline angle of 44.3° which corresponds to its experimental value averaged in the range $x/c = 0.47 - 0.75$.

In the flow disturbed by the elongated roughness element installed on the wing surface, two vortices are generated, that is, Vortex 1 and Vortex 2 originating at the left-hand and the right-hand sides of the element, respectively. Spaced in the spanwise direction, they seem to develop without significant interaction with each other. The stationary perturbations of the base flow induced by these vortices are shown as 3D plots in Fig. 3; in this and the following figures, the results obtained for the streamwise component of the flow perturbations are presented.

Then, to examine secondary instabilities, harmonic oscillations were forced at the frequency of 210 Hz which was close to the spectral maximum of the high-frequency perturbations observed at their natural growth in the boundary layer modulated by the primary vortices. The disturbances were excited at low levels of the periodic forcing so that linear oscillations with rather small initial amplitudes were induced at the position of their generator. Evolution of the controlled secondary disturbances is illustrated in Fig. 4. The oscillations appear as oblique waves at their spatial arrangement most likely dominated by interplay of the 3D boundary layer with the stationary vortices. As is seen, they are transported in narrow regions of the base-flow distortion (compare to Fig. 3) and well periodic in the major part of the measurement domain. According to Fig. 4, streamwise propagation velocity of the perturbations makes about 0.55 of the external-flow, which is typical for the oscillations in swept-wing boundary layers. The disturbances convected away

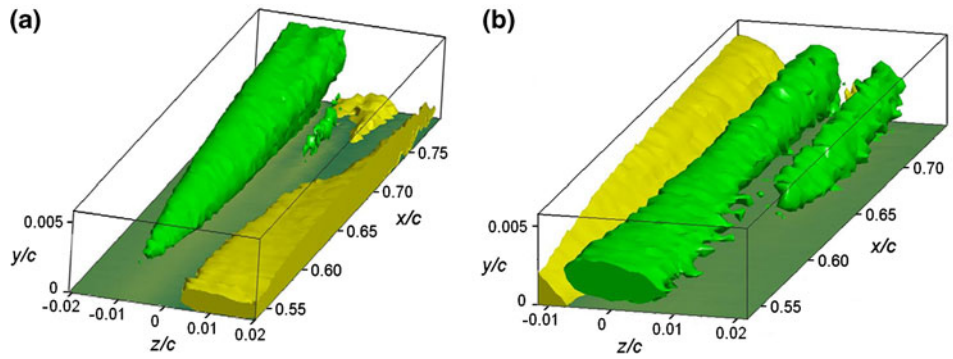


**Fig. 3** Stationary boundary-layer disturbances generated by the 35-mm roughness element, amplitude levels are −6% (*green*) and +6% (*yellow*) of $U_0$. **a** Vortex 1, **b** Vortex 2

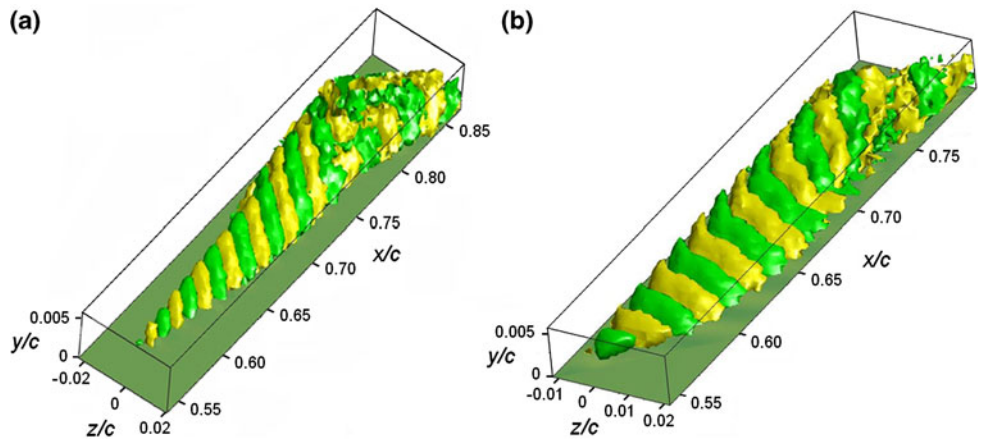


**Fig. 4** Secondary oscillations behind the 35-mm roughness element, amplitude levels are ±0.5% (*green* and *yellow*) of $U_0$. **a**, **b** High-frequency perturbations with their maximum amplitudes $u'/U_0$ in the reference section $x/c = 0.58$ as high as 0.8 and 1.5% riding on Vortex 1 and Vortex 2, respectively

from the generator amplify and finally result in chaotic motion. The periodicity of the oscillations is masked in the aft part of the boxes shown in Fig. 4 by small-scale irregularities, testifying to a broad spectrum of velocity fluctuations.

When changing the elongated roughness element to the circular one, the amplitude of the stationary perturbation measured at $x/c = 0.58$ was found to decrease almost three times. Apparently, at diminution of the spacing between the counter-rotating vortices, they interfere with each other so that the induced base-flow modulation gets weaker. Thus, it is expected that mean-velocity gradients generated by the vortices become smaller and the boundary layer is stabilized to the high-frequency disturbances. An indication on suppression of the secondary instability at the vortices interaction, which is followed by a delay of the laminar-flow breakdown, is given in Fig. 5. One can see that in this case, the high-frequency disturbances do not evolve into 3D irregular structures so that their coherence is found in the entire domain (compare to Fig. 4).

More distinctly, the effect of the vortex configuration on the secondary perturbations is seen in Fig. 6 where growth curves of the oscillations at the excitation frequency are plotted. The boundary layer modulated by Vortex 1 is the most unstable. The secondary instability of Vortex 2 is somewhat lower, as one can find comparing the amplification rates at $x/c \leq 0.65/0.70$, which is due to different mean-flow perturbations produced by the isolated vortices of opposite rotation. In both the cases, however, the disturbances still grow almost at the same rate in the right-hand sections of Fig. 6 where the laminar-flow breakdown is observed (see Fig. 4). In contrast, the secondary oscillations become almost neutral and even decaying with the streamwise distance at the primary vortices interaction.

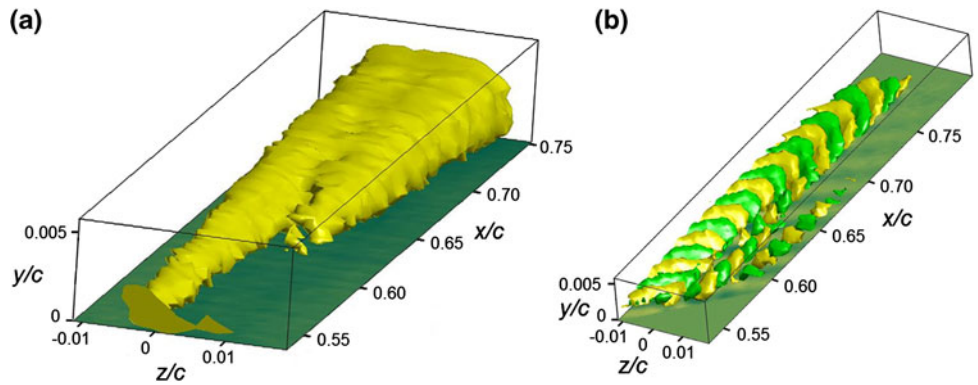


**Fig. 5** Boundary layer perturbed by the circular roughness element. **a** Stationary disturbance and **b** secondary oscillations with $u'/U_0 = 0.4\%$ at $x/c = 0.58$, amplitude levels are $+1.2\%$ and $\pm 0.1\%$ of $U_0$, respectively

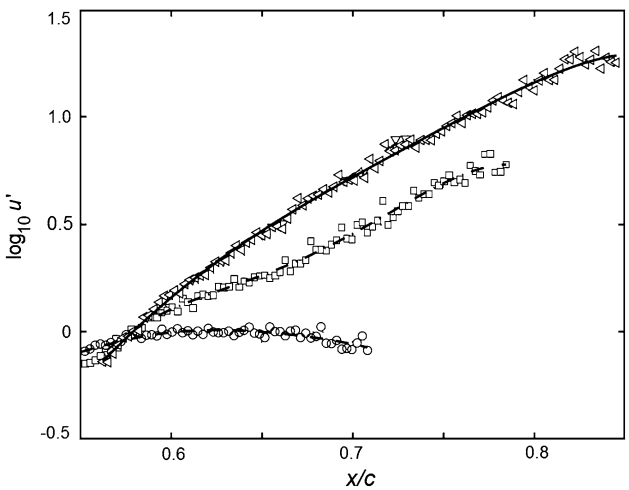


**Fig. 6** Maximum amplitudes of the high-frequency oscillations reduced by their values at $x/c = 0.58$ in the cases of Vortex 1 (*triangles*), Vortex 2 (*squares*) and the interacting vortices (*circles*); *lines* are polynomial data fit

## 4 Conclusion

The results of this study illustrate a pronounced effect, which may have spatial arrangement of the stationary vortices in a swept-wing boundary layer on the laminar-flow breakdown. As is shown, the behavior of secondary perturbations involved in transition to turbulence is quite different depending on transverse spacing of the primary base-flow disturbances. That is, amplification of the secondary oscillations is obviously reduced when the isolated counter-rotating vortices start to interact, approaching each other.

Under natural conditions, the primary 3D boundary-layer instability, appearing in the form of stationary crossflow vortices, is excited by background disturbances, e.g. surface roughness inherent to wall-bounded flows in a variety of applications. At the same time, controlled (discrete) roughness elements can be used for the transition delay in a swept-wing flow through their effect on the boundary-layer instability (Carpenter et al. 2009). The present experimental data give an illustration on modification of the transitional flow characteristics which could be achieved with controlled roughness elements of a proper configuration, modulating the primary boundary-layer perturbations and their secondary instabilities.

**Acknowledgments** V.V.K. would like to thank Chalmers University of Technology for hosting him during his research visits when this work was carried out. The present study was also supported by President of Russian Federation (NSh-454.2008.1), the Russian Foundation for Basic Research (Grant No 08-01-00027) and the Ministry of Education and Science of Russian Federation (Project RNP 2.1.2.541).

## References

Boiko AV, Kozlov VV, Sova VA, Scherbakov VA (2000) Generation of streamwise structures in a boundary layer of a swept wing and their secondary instability. Thermophys Aeromech 7:25–35

Carpenter AL, Saric WS, Reed HL (2009) Roughness receptivity studies in a 3-D boundary layer—flight tests and computations. In: Seventh IUTAM symp. on laminar–turbulent transition, book of abstracts. Royal Institute of Technology, Stockholm, pp 120–121

Deyhle H, Bippes H (1996) Disturbance growth in an unstable three-dimensional boundary layer and its dependence on environmental conditions. J Fluid Mech 316:73–113

Elofsson P, Kawakami M, Alfredsson P (1999) Experiments on the stability of streamwise streaks in plane Poiseuille flow. Phys Fluids 11:915–930

Fischer TM, Dallmann U (1991) Primary and secondary stability analysis of a three-dimensional boundary-layer flow. Phys Fluids A 3:2378–2391

Högberg M, Henningson D (1998) Secondary instability of crossflow vortices in Falkner–Skan–Cooke boundary layers. J Fluid Mech 368:339–357

Janke E, Balakumar P (2000) On the secondary instability of three-dimensional boundary layers. Theor Comput Fluid Dyn 14:167–194

Kawakami M, Kohama Y, Okutsu M (1999) Stability characteristics of stationary crossflow vortices in three-dimensional boundary layer. AIAA Paper 99-0811

Koch W (2002) On the spatio-temporal stability of primary and secondary crossflow vortices in a three-dimensional boundary layer. J Fluid Mech 456:85–111

Koch W, Bertolotti F, Stolte A, Hein S (2000) Nonlinear equilibrium solutions in a three-dimensional boundary layer and their secondary instability. J Fluid Mech 406:131–174

Kohama Y, Saric W, Hoos W (1991) A high-frequency, secondary instability of crossflow vortices, that leads to transition. In: Proc. RAS conf. on boundary-layer and control, Cambridge, pp 4.1–4.13

Kohama Y, Onodera T, Egami Y (1996) Design and control of crossflow instability field. In: Duck P, Hall P (eds) IUTAM symp. on nonlinear instability and transition in three-dimensional boundary layers. Kluwer, Manchester, pp 147–156

Kozlov V, Sova V, Shcherbakov V (2001) Experimental investigation of the development of secondary perturbations on a swept wing. Fluid Dyn 36:909–914

Malik M, Li F, Choudhari M, Chang C-L (1999) Secondary instability of crossflow vortices and swept-wing boundary-layer transition. J Fluid Mech 399:85–115

Matsson O, Alfredsson P (1990) Curvature- and rotation-induced instabilities in channel flow. J Fluid Mech 210:537–563

Matsubara M, Alfredsson P (2001) Disturbance growth in boundary layers subjected to free-stream turbulence. J Fluid Mech 430:149–168

Nitschke-Kowsky P, Bippes H (1988) Instability and transition of a three-dimensional boundary layer on a swept flat plate. Phys Fluids 31:786–795

Poll DIA (1979) Transition in the infinite swept attachment line boundary layer. Aeronaut Q 30:607–629

Saric W, Reed H, White E (2003) Stability and transition of three-dimensional boundary layers. Annu Rev Fluid Mech 35:413–440

Wassermann P, Kloker M (2002) Mechanisms and passive control of crossflow-vortex-induced transition in a three-dimensional boundary layer. J Fluid Mech 456:49–84

White E, Saric W (2005) Secondary instability of crossflow vortices. J Fluid Mech 525:275–308

White E, Saric W, Gladden R, Gabet P (2001) Stages of swept-wing transition. AIAA Paper 2001-0271